Water Practice & Technology

IWA PUBLISHING

Water Practice & Technology Vol 18 No 5, 1051 doi: 10.2166/wpt.2023.068

Potential of *Citrus limetta* peel powder (CLPP) for adsorption of hazardous Congo red dye from wastewater

Ujala Aslam and Tariq Javed*

Department of Chemistry, University of Sahiwal, Sahiwal, Punjab 57000, Pakistan
*Corresponding author. E-mail: mtariq@uosahiwal.edu.pk

ABSTRACT

In this study, Congo red anionic dye was removed from an aqueous solution using powdered *Citrus limetta* peel. The adsorbent was evaluated with the use of FTIR and SEM. The highest dye removal was achieved when the operating parameters were optimized, including pH = 6.0, adsorbent dose = 0.4 g, contact time = 90 min, initial adsorbate conc. = 10 ppm, and temperature = 60 °C. The pseudo-second-order model was investigated to have the best fit for the kinetics of the process, with $R^2 = 0.9918$ and $Q_{e(cal)} = 0.206$ mg g^{-1}, which is very close to the experimental $Q_{e(exp)} = 0.191$ mg g^{-1}. These two models' plots showed that both physical and chemical adsorption were feasible. ΔG and ΔH being negative suggest that the adsorption was thermodynamically favorable and spontaneous. Testing the suggested technique with groundwater resulted in an 82% CR adsorption efficiency. Due to the incredible removal capacity of CR dyes from industrial effluents, research suggests that CLPP can be used as substitute adsorbents for the treatment of wastewater from the weaving and dyeing industries.

Key words: adsorption, *Citrus limetta* peel powder, Congo red, thermodynamics

HIGHLIGHTS

- *Citrus limetta* peel powder is cheap, effective and potential adsorbent for Congo red adsorption from wastewater.
- The protonated part of hydroxyl and carboxyl group of CLPP combine with negative part of Congo red dye for adsorption of dye molecules.
- Adsorbent characterization, optimized parameters, and adsorbent recovery were studied.
- Kinetics, isotherm models, and thermodynamics were evaluated.

GRAPHICAL ABSTRACT

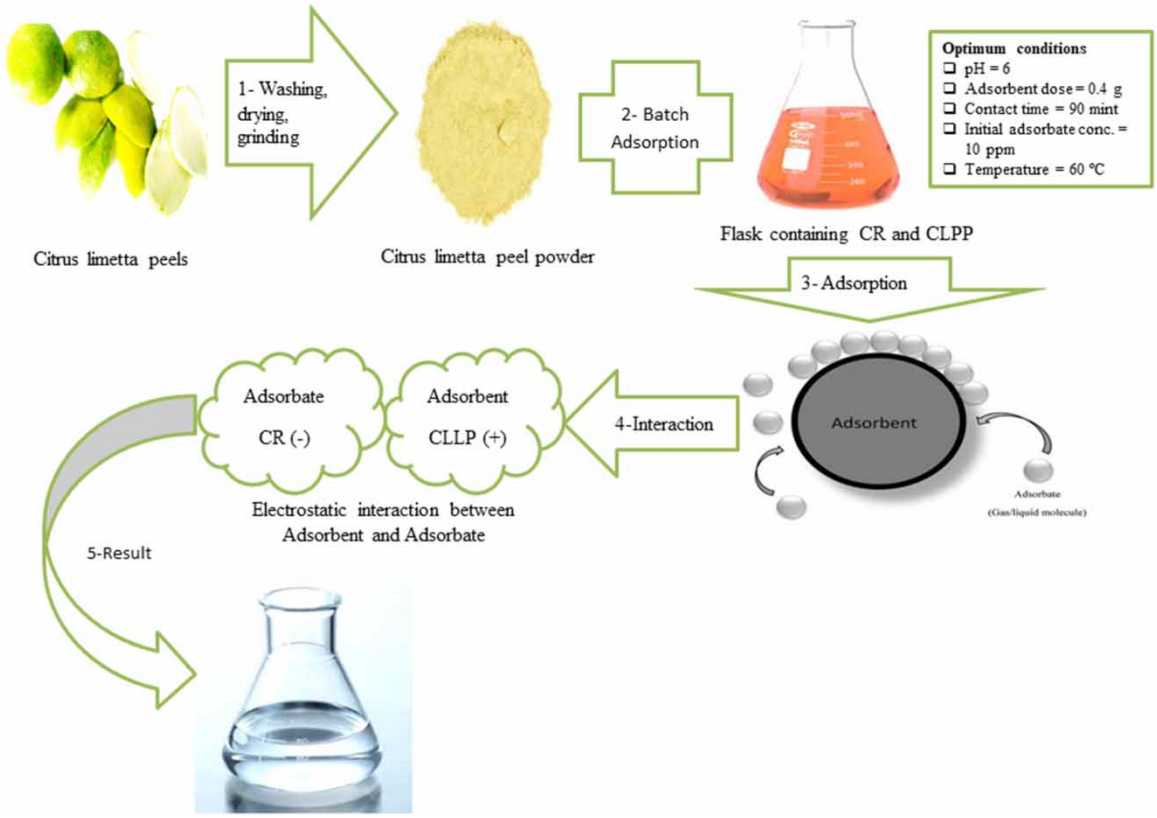

1. INTRODUCTION

The availability of fresh, clean drinking water decreases as the population is increasing. It is impossible to overstate the importance of water for human consumption. The solubility of all contaminants or solutes makes water quality gradually decrease (Wang & Chu 2011; Imran *et al.* 2022). Water pollution causes worldwide harmful diseases and kills about 15,000 people every day. As a result, the first logical step in solving this enormous issue is the recovery of clean water from wastewater. According to the World Bank, the textile business is one of the most polluting industries on the planet (Khan & Malik 2014). The Comprehensive Regulation of Contaminant Services Regulations of South Korea, which is applicable to both water and air pollution, identifies workplaces that produce more than 80 tons of air pollutants annually or more than 2,000 m^3 of water pollutants daily (Kim *et al.* 2022). It is common knowledge that dumping dyes into waterways lowers sunlight penetration, boosts biological (BOD) and chemical (COD) oxygen consumption, slows respiration, and restricts plant growth (Al-Tohamy *et al.* 2022). Synthetic dyes are resistant, bioaccumulative, poisonous, mutagenic, and carcinogenic substances (Lellis *et al.* 2019).

The adsorbate that has to be extracted from water is Congo red (CR; Figure 1). It is a particular anionic dye. It produces a blue-colored solution in an aqueous media when the pH is below or equivalent to 3, and becomes red when the pH is above 5 (Wang & Wang 2008). Its chemical formula is $C_{32}H_{22}N_6\ Na_2O_6S_2$. The molar mass of CR is 696.665, $\lambda_{max} = 496$ nm, 497 nm.

CR was formerly used to color fabrics, but lighter, stain-resistant dyes have now replaced it. It is still used in histology to stain tissues for microscopic study and as an acid-base indicator since it turns red in the presence of alkalies and blue in the presence of acids (Swan & Zaini 2019). Along with similar dyes from the textile, printing and dyeing, paper, rubber, and plastic sectors, it is a serious effluent concern. Consequently, CR has been prohibited because of its cancer-causing properties (El-Ahmady *et al.* 2020).

For the decolorization of effluents, different kinds of processes are available, including ozonation, membrane separation, coagulation/flocculation, co-precipitation, oxidation, electrolysis, microorganism degradation, photochemical, and adsorption employing various types of adsorbents (Sharma & Kaur 2018; Samsami *et al.* 2020). Because it is a cheap method for extracting pigments or decolorizing textile pollutants, adsorption has been

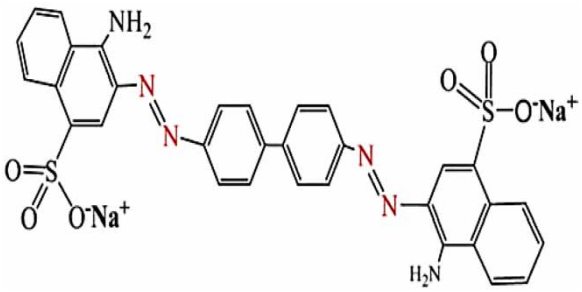

Figure 1 | Structure of Congo red.

found to be one of the most successful and established wastewater treatment processes in the textile industry (Chai *et al.* 2021), Agricultural wastes such as rice husk (Chuah *et al.* 2005), sugarcane (Sarker *et al.* 2017), orange peel (Alwared *et al.* 2021), banana peel (Akpomie & Conradie 2020), dried neem leaf (Bhattacharyya & Sharma 2004), and corncobs (Peñafiel *et al.* 2020), as well as byproducts such as sugarcane husk, bamboo sawdust, moss, mud, kaolin, red soil, alumina, leaf extract, wood pellets, powdered peanut shells powder, and other lingo-cellulosic wastes have been used to study biosorption (Sharma & Kaur 2018), The benefits of adopting these materials include their widespread availability and inexpensive cost, as well as the fact that they do not require regeneration.

Citrus limetta is mainly used for the purpose of making juice, and the peels are dumped as garbage. These peels can be used for biosorption. Biochar from the peels of sweet lemon has been used for the extraction of dyes from wastewater (Shakoor & Nasar 2016, 2018). The novelty of this article is studying the feasibility of *C. limetta* peels, which is cost-effective and easily available as an adsorbent in decolorizing CR dye from textile industries. The objective of this study was to identify the answers to the following questions: What is the fundamental process through which CR dye adheres to C. limetta peel? What characteristics of the *C. limetta* peel are responsible for wastewater decolorization? The adsorption ability of *C. limetta* peel was lastly compared with that of other adsorbents used in the adsorption of CR dye. There are no boundaries to study, and this work creates a connection as well as the relationship between the experiential framework and the application of these adsorbents for the adsorption of dyes from effluent. The complete process of the current research is as follows (Figure 2):

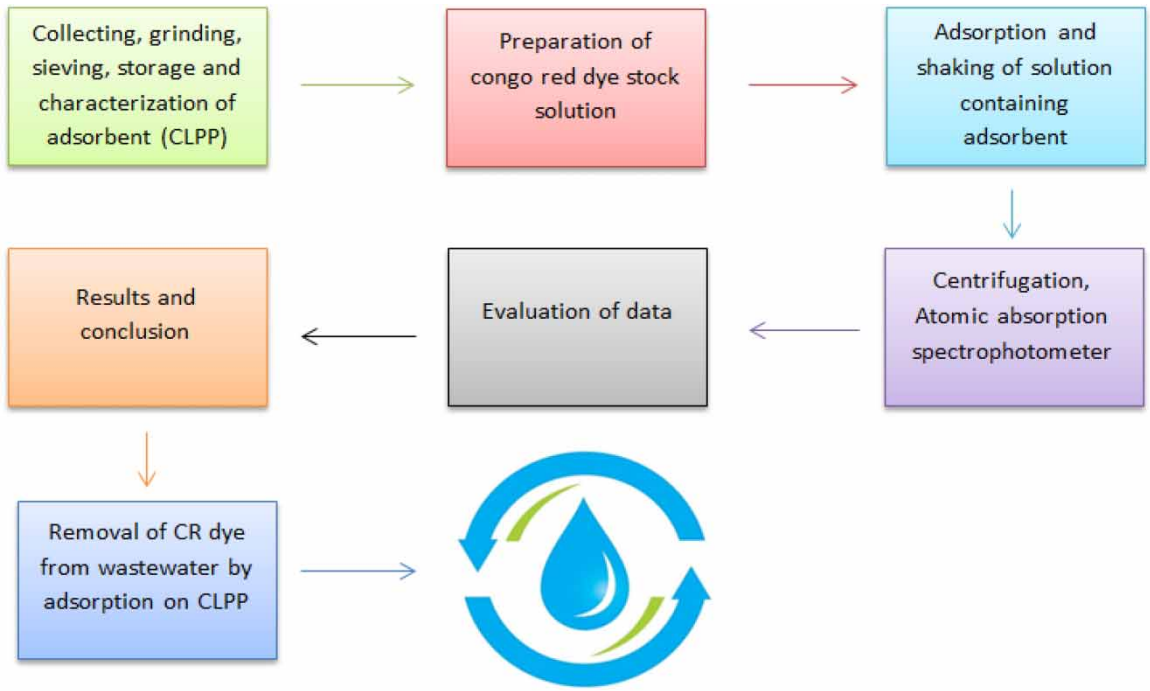

Figure 2 | Scheme of adsorption of Congo red onto *Citrus limetta* peels.

2. EXPERIMENTATION AND METHODS

2.1. Chemicals and equipment

Nitric acid (HNO_3) and sodium hydroxide (NaOH) were utilized as chemicals in the research studies, while deionized water was used throughout the study. UV–Vis spectrophotometer, scanning electron microscope (SEM), Fourier-transform infrared (FTIR) spectrophotometer, centrifugation machine, microwave, pH meter, weighing machine, conical flasks, beakers, pipettes, and a hot plate are all required during the entire procedure.

2.2. Preparation of CR dye solution

CR dye with a molecular formula $C_{32}H_{22}N_6\ Na_2O_6S_2$ and molar mass of 696.665 g mol^{-1} was collected from a chemistry laboratory, and to make 1,000 mg g^{-1} dye stock solutions, CR was dissolved in 500 ml of deionized water, and the solution was then further diluted as needed.

2.3. Collection of adsorbents

C. limetta peel was obtained from a local market and was then dried and crushed into little granular particles (Figure 3) to maximize its surface area. Particles of varied sieve sizes, including 105, 210, and 500 μm, were extracted via sieving and then kept in sealed storage containers for subsequent research.

Figure 3 | *Citrus limetta* dried peel and peel powder.

2.4. Adsorption batch studies

Batch adsorption analyses were utilized to optimize a number of adsorption characteristics, including temperature (0, 10, 20, 30, 40, 50, and 60 °C), initial concentration of adsorbate CR dye (5, 10–100 ppm), amount of adsorbent (*C. limetta* peel powder; CLPP) dose (0.1–1.0 g), and pH (1–12). Throughout the experiments, just one adsorption parameter was adjusted at a time, keeping the others unchanged. After shaking, centrifugation was performed, and the quantity of CR dye contained in the sample solution was quantified by measuring absorbance at 496 nm using a UV–Vis spectrophotometer.

The percentage dye removal formula was given in the following equation:

$$\%\ \text{removal} = \frac{A_i - A_f}{A_i} \times 100 \tag{1}$$

where A_i is the initial absorbance before dye adsorption and A_f is the final absorbance after dye adsorption. Adsorption capacity q_t (mg g^{-1}) was determined by the formula given in the following equation:

$$q_t = \frac{(C_0 - C_e)V}{M} \tag{2}$$

where C_0 (mg L^{-1}) is the initial concentration, C_e (mg L^{-1}) is the equilibrium concentration of dye, V is the volume taken for the dye solution; and M is the adsorbent's molar mass.

2.5. Identification of pH_{pzc}

45 mL of 0.1 M KNO_3 solutions were taken in several 100 mL conical flasks to identify the point of zero charge pH_{pzc} of the adsorbent, and 1 g of the adsorbent was added to each flask in a range of 1–12. Now, 0.1 M HCl/NaOH solutions were used to adjust the pH_i values of these solutions in the range of 1–12. Each flask's total amount of solution was exactly 50 mL. After 2 days, the final pH of the liquids in these flasks was tested. The difference between initial pH and final pH values ($\Delta pH = pH_i - pH_f$) was plotted against initial pH. The junction point of the curve of ΔpH versus $pH_{initial}$ was noted as pH_{pzc} of the CLPP.

3. CHARACTERIZATION OF ADSORBENT

3.1. FTIR spectroscopy analysis

Using a Perkin Elmer FTIR spectrophotometer, the position of different functional groups (located at the surface of CLPP) was identified. The FTIR analysis of the adsorbent was carried out using a 100 mg pallet of potassium bromide (KBr) with a spectrum range of 4,000–600 cm^{-1} (Tiernan *et al.* 2020).

3.2. Scanning electron microscopy (SEM) analysis

The adsorbent was investigated using an SEM both before and after adsorption (JEOL, JSM-6510LV, Japan). In order to eliminate the hazardous CR dye, the morphological characteristics and texture of *C. limetta* were determined by using an SEM.

4. RESULTS AND DISCUSSION

4.1. FTIR analysis of CLPP

FTIR spectroscopy was used to identify different functional groups that were present on the CLPP adsorbent's surface. Figure 4 presents the FTIR spectrum of CLPP before and after CR adsorption. The existence of hydroxyl groups (–OH) in C. limetta peel was mostly attributable to a wide band appearance of about 3,337 cm^{-1} in the FTIR spectra. The peak at 2,917 cm^{-1} was attributed to methylene group C–H stretching. The CO bond of the carboxylic groups found in the parts of biosorbent (CLPP) was ascribed to the strong peaks at 1,690 and 1,647 cm^{-1} (Nandiyanto *et al.* 2019). The ring of aromatic molecules might be responsible for the peaks at 1,453 and 1,421 cm^{-1}. The CH group on the surface of the CLPP is referred to the band at 1,377 cm^{-1}. The peak at 1,183 cm^{-1} refers to an irregular length of the COC ether group found in the CLPP surface. The CO stretch of primary alcohol is responsible for the band's appearance at 1,037 cm^{-1} (Oyekanmi *et al.* 2021). Some shifts (8 to 22 cm^{-1}) were identified in the FTIR spectra of Figure 4, which correspond to the OH and COOH groups, showing that these compounds noticeably improve the adsorption of Congo red dye onto the powdered *C. limetta* peels. Small changes in other frequencies are also observed. Functional groups such as –OH, –COOH, $-C=O$, $-C_6H_6$, and aliphatic stretching were identified on the adsorbent surface, as shown in Table 1.

4.2. SEM analysis of CLPP

C. limetta peels were estimated to have an average particle size of less than 1 mm. SEM investigations were performed on blank *C. limetta* peels and CR dye loaded *C. limetta* peels for structural and morphological properties (Figure 5). *C. limetta* peel SEM analysis revealed a great number of holes on the surface, as well as fissures and crevices. The surface modification of CR dye loaded *C. limetta* peels resulted in variations in morphology, such as surface structure (few pores are filled) (Buvaneswari & Singanan 2020).

4.3. Effect of pH

The surface characteristics of the adsorbent, in addition to the extent of dye molecule ionization, are altered by the initial pH of the dye solution. Therefore, it is essential to inquire into how pH affects the adsorption process. Figure 6(a) illustrates the impact of the initial pH on the quantity of dye solution absorbed by the C. limetta peel samples. 100 ml of 10 ppm CR dye solutions with a pH range of 1–12 were produced for this experiment. The pH of the solutions was adjusted using a pH meter or strip by adding 0.1 N sodium hydroxide (NaOH) and 0.1 N hydrochloric acid (HCL) solutions. 0.25 g of 105 μm mesh size adsorbent was added to each of the solution, stirred vigorously for 5 min and then allowed to stand room temperature (20 °C) for 20 min. The final dye concentration in the supernatant solution was assessed using a visible spectrophotometer at 496 nm after the solution had been incubated for 20 min. The % removal of dye at each pH value was calculated using

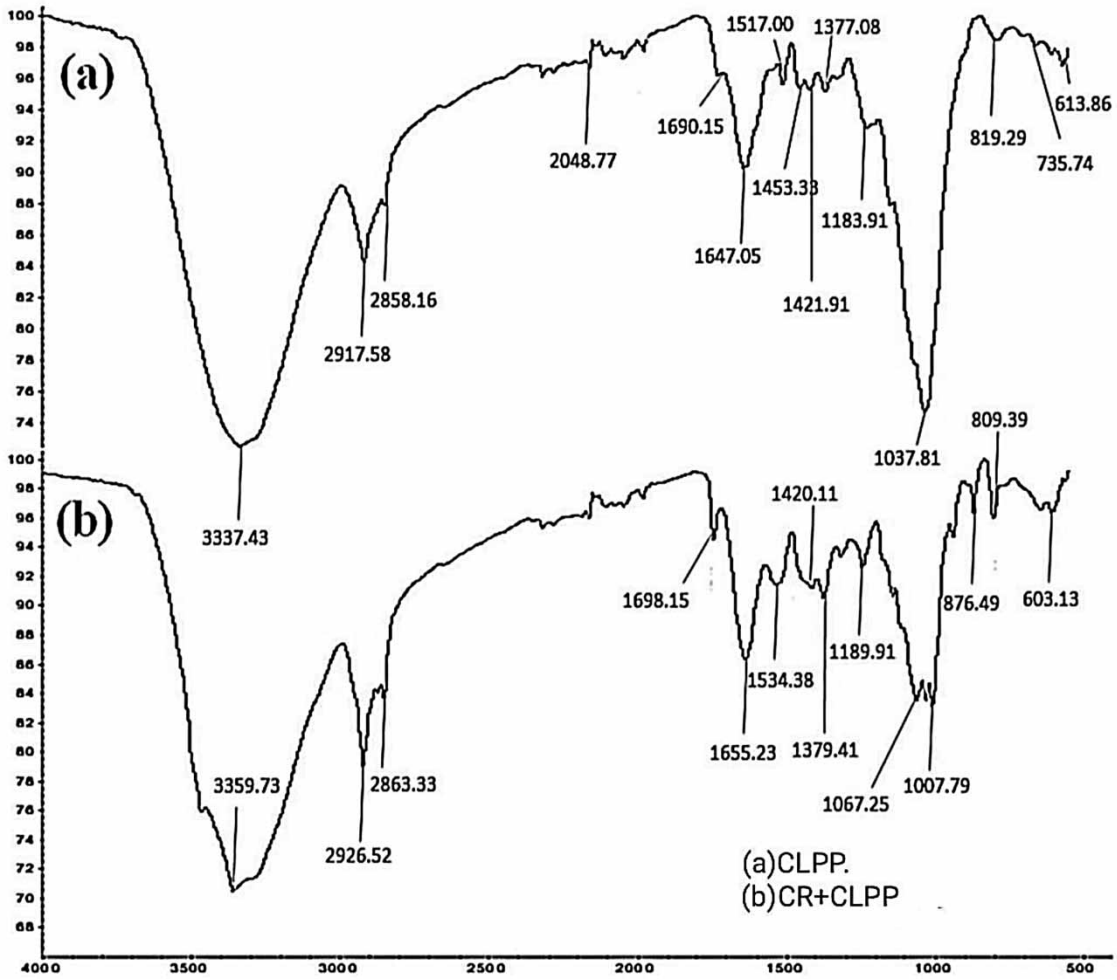

Figure 4 | FTIR spectrum of Congo red dye before adsorption (a) and after adsorption (b) (Oyekanmi *et al.* 2021).

Table 1 | FTIR spectrum analysis of CLPP

FTIR peak of CLPP (cm^{-1})	Assignment
3,337	O–H
2,917	CH_3/C–H asymmetric stretching vibration
1,690, 1,647	C–O stretching of carboxylic bond
1,453 and 1,421	Aromatic compound
1,377	C–H groups
1,183	C–O–C asymmetric stretching
1,037	C–O stretching of alcohol

Equation (1). The result given in Figure 6(a) demonstrates that dye removal efficiency in pH 6 is relatively high. The interactions between positively charged dye cations and surface functional groups present in mosambi peels might explain the increased adsorption in acidic conditions. The adsorption decreases at higher pH levels, which might be due to the production of soluble hydroxyl complexes (Guo *et al.* 2020; Karaman *et al.* 2022). According to the experimental findings (shown in Supplementary Table S1), dye absorption was decreased in extremely acidic condition (14.43% at pH 1).

The point of zero charge (pH_{pzc}) provides the best explanation for how pH solution affects dye absorption. As a consequence of pH, it is an advantageous and useful surface characteristic for identifying whether the surface is

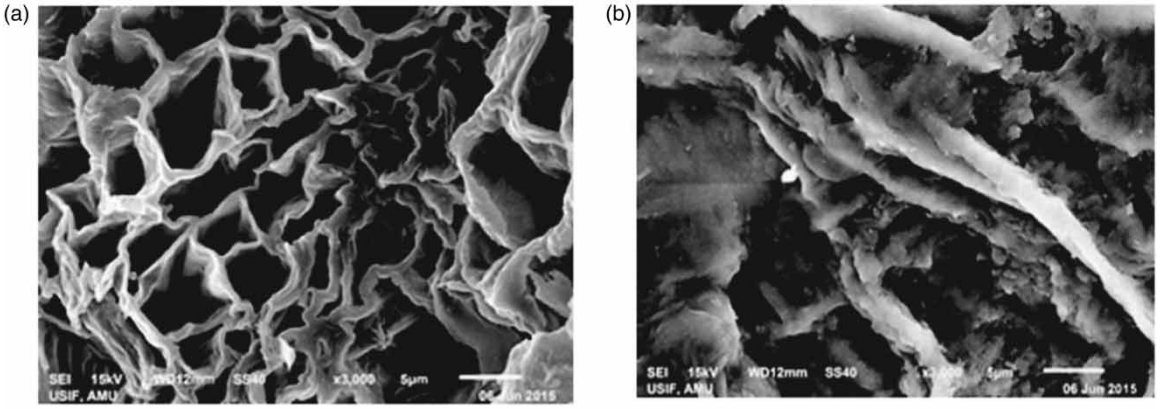

Figure 5 | SEM image of CLPP biomass (a) biomass loaded with CR (b) (Reproduced with permission from Shakoor & Nasar (2016)).

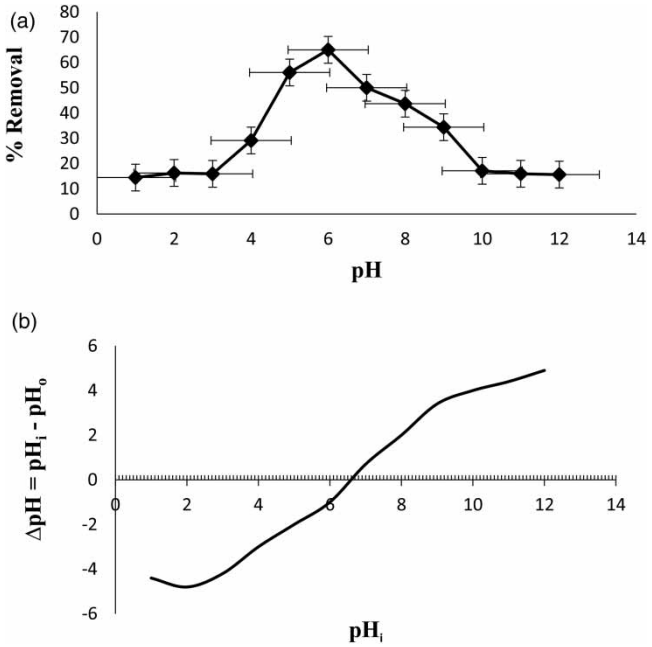

Figure 6 | (a) Effect of pH on adsorption of CR using CLPP. (b) Graph for determination of point of zero charge (pH_{pzc}).

positively or negatively charged. The point of zero charge (pH_{pzc}) value for CLPP was 6.6 (Figure 6(b)). This indicates that the adsorbent (CLPP) surface is positively charged at pH values below 8, net zero at pH 8, and negatively charged at pH values above 8. So, any anionic dye, like CR, is better able to adhere to the surface of the CLPP in a solution with a pH lower than 8. Due to the electrostatic force of attraction, the surface of the CLPP adsorbent becomes positively charged, which enhances the absorption of anionic dye. The removal of anionic dyes tartrazine and methyl blue yielded similar results (Ali *et al.* 2022; Rani & Chaudhary 2022).

4.4. Effect of adsorbent dose

For the varied amount of dosages of 0.1, 0.2, 0.4, 0.6, 0.8, and 1.0 g in a solution of volume 10 ml, the effects of the adsorbent, i.e., CLPP dose, on the quantity of dye adsorption expressed as a percentage at an initial concentration of 10 mg L^{-1} at 20 °C were studied. Figure 7 shows that as the adsorbent dose is increased, the percentage of dye removal increases until the quantity of dye removal is no longer increased up to a certain limit (i.e., 0.4 g), after which it becomes constant because dye molecules have taken up all of the active sites (Lafi *et al.* 2019; Guo *et al.* 2020). The cause of this might be linked to interparticle attraction or the loss of open surface area due to congestion. The results of the experiment are given in Supplementary Table S2.

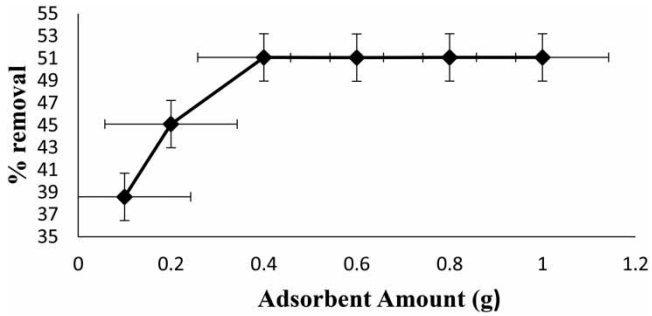

Figure 7 | Effect of adsorbent dose on adsorption of CR using CLPP.

4.5. Effect of contact time

At 10 ppm initial CR concentrations, the effect of contact time of CLPP adsorption capacity was investigated. The adsorption capacity rises with contact time and attains equilibrium after 90 min, as shown in Figure 8. It mostly originates from the presence of these binding sites on the powdered *C. limetta* peel that hinders any additional adsorption. This may be due to the fact that there are initially quite enough sites on the surface, which makes adsorption relatively simple. However, as time passes, the adsorbent surface gets saturated, slowing down the rate of adsorption (Suryavanshi & Shukla 2010). However, within the first 50 min, the rise is relatively higher. Experimental results are given in Supplementary Table S3.

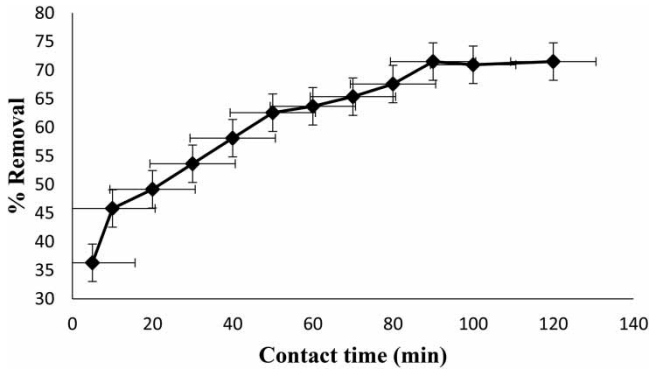

Figure 8 | Effect of contact time on adsorption of CR onto CLPP.

4.6. Effect of initial dye concentration

In the initial concentration range of 5–100 ppm, the effects of adsorbate concentration on adsorption effectiveness were studied. Results showed that when the initial dye concentration is increased from 10 to 100 ppm, the adsorption capacity of CLPP seems to decrease at equilibrium. Figure 9 shows that a 0.4 adsorbent dosage of CLPP at 20 °C removed 73.01% of the dye at 10 ppm (Supplementary Table S4). Furthermore, if the dye concentration in the solution is lower, more dye molecules will encircle the active sites, resulting in more efficient adsorption (Rani & Chaudhary 2022).

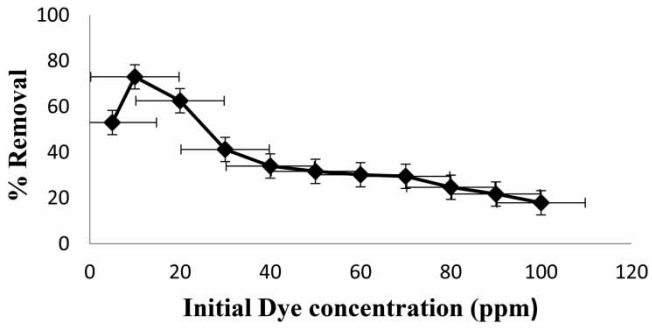

Figure 9 | Effect of initial dye concentration on adsorption of CR onto CLPP.

4.7. Effect of temperature

The impact of temperature on CR adsorption has been studied at optimum conditions. Figure 10 illustrates the CR adsorption by CLPP at different temperatures from 0 to 60 °C. The results depicted in Figure 10 clearly demonstrate that the percentage of CR removed was highest at 60 °C, at approximately 88.2% (result given in Supplementary Table S5). The temperature has no impact on the amount of dye that is reduced, but there is a substantial increase in adsorption, indicating that the interactions between CR dye and the adsorbent (CLPP) seem to be endothermic (Sahmoune 2019; Rani & Chaudhary 2022). The adsorption of CR dye molecules to the surface of CLPP at higher temperatures is related to strong binding forces.

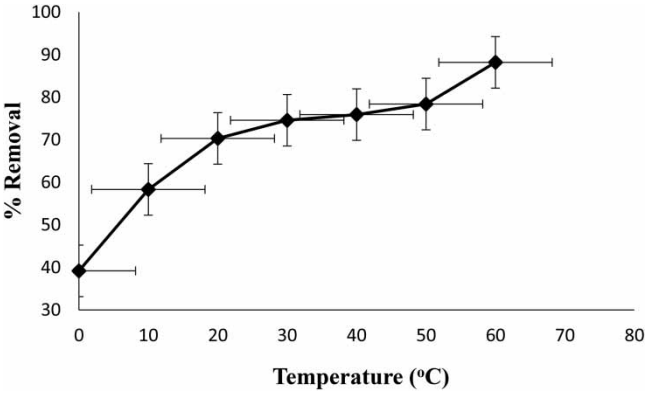

Figure 10 | Effect of temperature on adsorption of CR using CLPP.

4.8. Adsorption kinetic models

The adsorption kinetic model is crucial in regulating the effectiveness of the adsorption process and the rate at which adsorbate is taken up, which regulates the residence duration at the solid surface interface. The adsorption of CR was investigated using kinetic models: pseudo-first-order and pseudo-second-order, intraparticle diffusion model, and liquid film diffusion model (Wekoye *et al.* 2020).

4.8.1. Pseudo-first-order kinetic model

The dye sorption kinetics was predicted using a pseudo-first-order kinetic model. As described by the Lagergren rate equation, the pseudo-first-order model is shown as follows:

$$\log (Q_e - Q_t) = \log Q_e - \frac{k_1}{2.303} t \tag{3}$$

where k_1 is the pseudo-first-order rate constant, while Q_e and Q_t are the quantities (mol g^{-1}) adsorbed at equilibrium and at time t, respectively (min^{-1}). The slope and intercept of log $(Q_e - Q_t)$ against t may be used to compute the rate constants k_1 and Q_e. If the estimated and observed Q_e values are equal, the adsorption follows pseudo-first-order kinetics. The output of the pseudo-first-order kinetic model is shown in Supplementary Table S6, and Figure 11 displays its plot. Values of Q_e and k_1 were calculated from the intercept and slope of the straight line of the plot, respectively. Values of the slope coefficient (0.9585), $Q_{e(cal)}$ (5.8089),

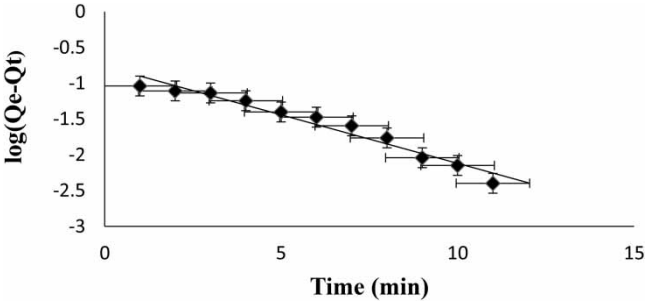

Figure 11 | Pseudo-first-order plot of CR removal onto CLPP.

and $Q_{e(exp)}$ (0.191) show that the dye's adsorption on CLPP did not follow a pseudo-first-order kinetic model, as there is a huge difference between these values (Yaneva & Georgieva 2012).

4.8.2. Pseudo-second-order kinetic model

The pseudo-second-order chemisorption kinetic rate equation is as follows if the rate of adsorption follows the pseudo-second-order mechanism:

$$\frac{t}{Q_t} = \frac{1}{k_2} + \frac{1}{Q_e} t \tag{4}$$

If the pseudo-second-order kinetic equation is valid, the plot of t/Q_t versus t should provide a straight line, from which the slope and intercepts may be used to get Q_e and k_2 (Felista *et al.* 2020). From the result (shown in Supplementary Table S7 and Figure 12), it indicates that the value of slope coefficient (0.9918) for the evaluation of the pseudo-second-order model is greater than that of the pseudo-first-order kinetic model, and a little difference between $Q_{e(exp)} = (0.191)$ and $Q_{e(cal)} = (0.20)$ values shows that data fits best to the pseudo-second-order kinetic model.

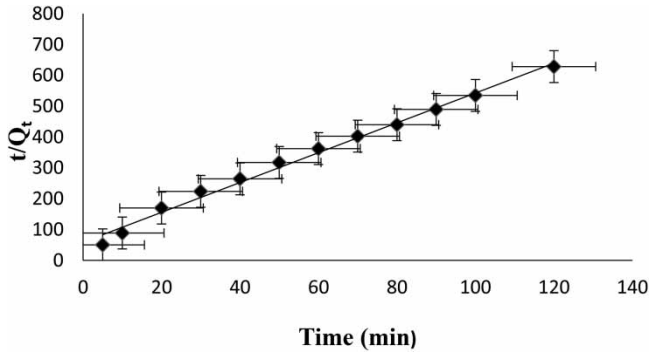

Figure 12 | Pseudo-second-order plot of CR removal onto CLPP.

4.8.3. Intraparticle diffusion model

The rate-determining step of the adsorption process is essential for the adsorption mechanism. Solute transmission is often identified by intraparticle diffusion, external mass transfer, or both. An intraparticle diffusion model based on the idea presented by Batool *et al.* (2021) was investigated to study the process of dye adsorption onto CLPP. This theory says that:

$$Q_t = K_{id} t_{0.5} + I \tag{5}$$

where Q_t denotes the quantity of dye adsorbed in (mg g^{-1}) at time t, I is the layer thickness, and K_{id} is the intraparticle diffusion constant in (mg $g^{-1}min^{1/2}$). A straight line is obtained by drawing a graph between Q_t and $K_{0.5}$ calculating the slope K_{id} and intercept 'I'. A linear plot indicates that the only model employed in the adsorption process is the intraparticle diffusion model, and a zero intercept indicates that this kinetic model is the rate-determining step.

The intraparticle diffusion model is not just a rate-determining step, as shown in Figure 13, but is also included in the control of the adsorption level when the line does not cross through the origin. This shows that the boundary layer is regulated to a somewhat extent (Silva *et al.* 2021). Supplementary Table S8 and Figure 13 present the graph and experiment's results, respectively. From the results, it was found that slope coefficient (R^2) value of the intraparticle diffusion model was 0.9795.

4.8.4. Liquid film diffusion model

The movement of adsorbate molecules through a liquid film that supports the solid adsorbent is considered to be the rate-determining step in the adsorption process.

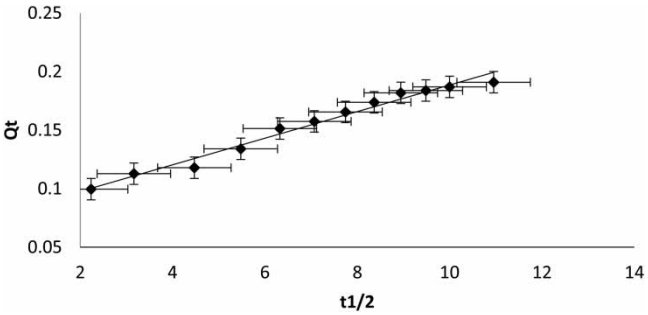

Figure 13 | Intraparticle diffusion plot of CR removal onto CLPP.

Mathematically, it may be expressed as follows:

$$\ln(1 - \mathrm{F}) = -k_{fd} \times t \tag{6}$$

where F is called fractional equilibrium attainment ($\mathrm{F} = Q_t/Q_e$) and k_{fd} (min^{-1}) is the film diffusion constant. The adsorption kinetics is regulated by diffusion through liquid film, according to a linear curve of –ln(1 – F) against time with zero intercept (Plazinski 2010). Supplementary Figure S9 depicts the experimental outcome plot. There is no evidence of linearity in the graph. $R^2 = 0.967$ is also less than unity. As a result given in Supplementary Table S9 and Figure 14, the liquid diffusion model is only partially applicable to the CR dye adsorption onto CLPP.

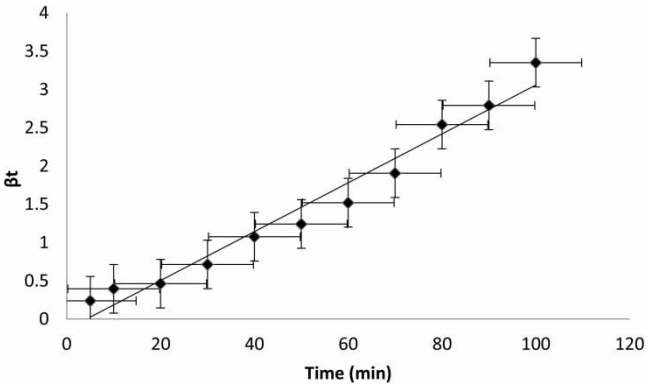

Figure 14 | Liquid film plot of CR removal onto CLPP.

Results from the intraparticle diffusion model, the pseudo-second-order kinetic model, the pseudo-first-order kinetic model, and the liquid film model are summarized in Table 2 in the appropriate order. Because it has the highest slope coefficient (0.9912) and closest to unity among the other models, the pseudo-second-order (PSO) kinetic model is used to explain the present adsorption process, as shown in Table 2. Furthermore, in the situation of the pseudo-second-order kinetics, there is a clear consensus between calculated and experimental Q_e ($\mathrm{mg\ g}^{-1}$) demonstrating that the data fits well with the pseudo-second-order model.

4.9. Adsorption isotherms

The adsorption process must be completely quantified before it can be used commercially. These mathematical models explain the interactions between the adsorbent and the adsorbate, as well as the adsorption capacity. The most suitable isotherm model in the adsorption process is done by analyzing concentration data from tests utilizing several isotherm models. Langmuir, Freundlich, D-R, and Temkin isotherms for CR adsorption onto CLPP adsorbent were used in this study.

Table 2 | Results of all discussed kinetic models

Kinetic models	Parameters	Values
Pseudo-first-order	k_1	0.312 min^{-1}
	$Q_{e(exp)}$	0.191 mg g^{-1}
	$Q_{e(cal)}$	5.808 mg g^{-1}
	R^2	0.9585
Pseudo-second-order	k_2	4.316×10^{-5} g $mg^{-1}min^{-1}$
	$Q_{e(exp)}$	0.191 mg g^{-1}
	$Q_{e(cal)}$	0.206 mg g^{-1}
	R^2	0.9912
Intraparticle diffusion model	K_{id}	0.0114 $min^{0.5}$
	R^2	0.9795
Liquid film model	K_{id}	0.0319 min^{-1}
	R^2	0.967

4.9.1. Langmuir isotherm model

The solid adsorbent's capacity for adsorption is restricted. Only one molecule of a solute may interact with each active site, which is all identical (monolayer adsorption). The adsorbate molecules do not interact with one another (Chen 2015).

A non-linear form of the Langmuir isotherm's mathematical equation can be written as follows:

$$Q_e = \frac{K_L Q_L C_e}{1 + K_L C_e} \tag{7}$$

A linear form of the Langmuir equation is expressed in the following equation:

$$\frac{1}{Q_e} = \frac{1}{Q_{max}} + \left(\frac{1}{Q_{max} K_L}\right)\frac{1}{C_e} \tag{8}$$

where Q_L is the maximum monolayer adsorption capacities (mg g^{-1}); K_L is the Langmuir isotherm constant (L mg^{-1}); C_e is the equilibrium concentration (mg L^{-1}); and Q_e is the amount of adsorbate (mg g^{-1}).

$$\frac{C_e}{Q_e} = \frac{1}{Q_{max} K_L} + \frac{C_e}{Q_{max}} \tag{9}$$

When a graph is plotted between C_e (mg L^{-1})/Q_e (mg g^{-1}) and C_e (mg L^{-1}) from which slope and intercept may be calculated, a straight line is formed. The experiment's findings, which are presented in Supplementary Table S11 and Figure 15, show that the adsorption of CR onto CLPP proceeds favorably since the value of R^2 for the Langmuir isotherm was 0.9891 (almost one). The value of the adsorption capacity Q_o is 1.314×10^{-6} mg g^{-1} (given in Table 3). It demonstrated that, for monolayer adsorption, the energy of the initial layer of molecules adsorbed on the adsorbent's surface is substantially equivalent to the potential of heat (Batool *et al.* 2021) The separation factor (R_L, also known as the equilibrium factor), which describes the major characteristics of the Langmuir isotherm, indicates whether the adsorption process is favorable ($0 < R_L < 1$), unfavorable ($R_L > 1$), linear ($R_L = 1$), or irreversible ($R_L = 0$) (Batool *et al.* 2021).

$$R_L = \frac{1}{1 + K_L C_0} \tag{10}$$

where K_L(L mg^{-1}) is the Langmuir constant related to the adsorption's energy and C_0 (mol L^{-1}) is initial dye concentration. Values of R_L identifying the shape of isotherm were calculated by the Langmuir constant 'K_L' and adsorbate concentration. The experimental value of K_L is 6.56×10^{-10} L/mg. From K_L and C_{In}, we can determine R_L. From the results (Supplementary Table S10), it was observed that R_L values equal to 1 confirm the linear uptake of CR adsorption. When using non-linear equations to calculate isotherm values, Wavemetrices IGOR

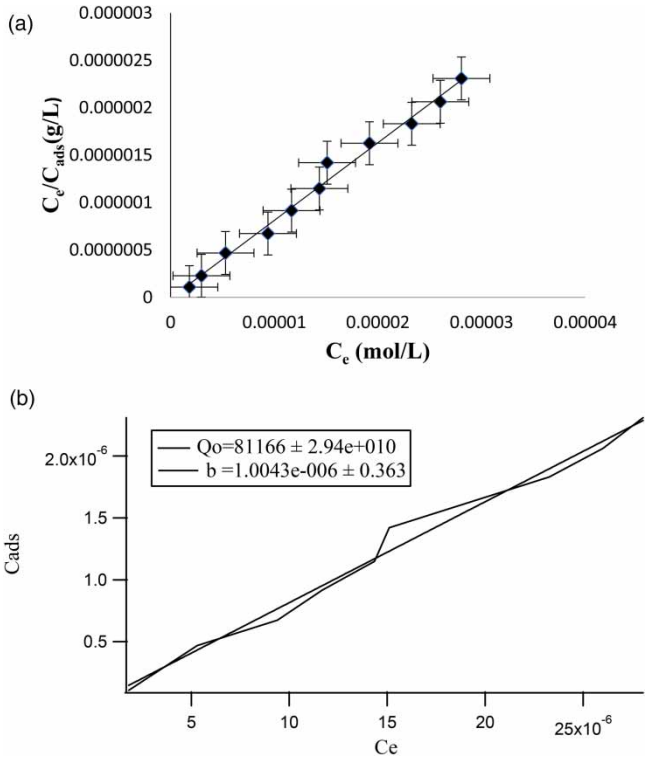

Figure 15 | (a) Langmuir isotherm's linear plot for removal of CR onto CLPP. (b) Langmuir isotherm's non-linear plot for removal of CR onto CLPP.

Table 3 | Parameters of adsorption isotherm models

Isotherm models	Parameters	Values
Langmuir isotherm	Q_o	1.314×10^{-6} mg g^{-1}
	K_L	6.56×10^{-10} dm mg^{-1}
	R^2	0.9891
Freundlich isotherm	N	1.9 L g^{-1}
	K_f	5.2742 mg g^{-1}
	R^2	0.9902
Temkin isotherm	B	8×10^{-7} J mol^{-1}
	A_T	1×10^{-5} L g^{-1}
	K_T	12.5
	R^2	0.885
D-R isotherm	B	-121.12 K J^2 mol^{-2}
	E_s	0.064K J mol^{-1}
	R^2	0.99

Pro 6.1.2 software was used (Zafar *et al.* 2019). Figure 15(b) demonstrates the Langmuir isotherm's non-linear model for CR dye adsorption onto CLPP.

4.9.2. Freundlich isotherm model

There are several kinds of energy adsorption sites, but they are all dispersed as a function of adsorption heat according to an exponential equation and share the same entropy. There is a linear reduction in the number of sites. The Freundlich isotherm model indicates that dye is adsorbed in several layers on the surface of heterogeneous adsorbents. The Freundlich equation may be expressed in linear form as follows:

$$\ln Q_e = \ln K_f + \frac{1}{n} \ln C_e \tag{11}$$

where Q_e (mg g^{-1}) is the quantity of adsorbate per unit adsorbent, K_f (mg g^{-1}) is the Freundlich constant where n is the slope, and C_e (mg L^{-1}) is the equilibrium concentration of CR dye in the solution. A straight-line graph is constructed by plotting ln Q_e versus ln C_e; the slope, $1/n$, gives us the value of n, and the intercept, ln K_f, gives us the value of K_f. When the value of 'n' is larger than one, more adsorption takes place (Anah & Astrini 2018; Felista *et al.* 2020). The value of n in the current study is 1.9 L g^{-1}, which is more than 1 and follows the Freundlich adsorption isotherm condition, i.e., $0 > n > 1$, showing that cooperative adsorption of CR dye on CLPP occurs to a significant extent. Good adsorption is indicated by a value of n between 2 and 10; moderate adsorption is represented by a value of n between 1 and 2; and poor adsorption is indicated by a value of n less than 1 (Imran *et al.* 2022; Sultana *et al.* 2022). The result of the Freundlich isotherm is presented in Supplementary Table S12, the Freundlich isotherm's linear plot is given in Figure 16(a), and the non-linear plot in Figure 16(b). The value of K_f in case of Freundlich isotherm was 5.2742 and that of R^2 was 0.9902 very close to unity.

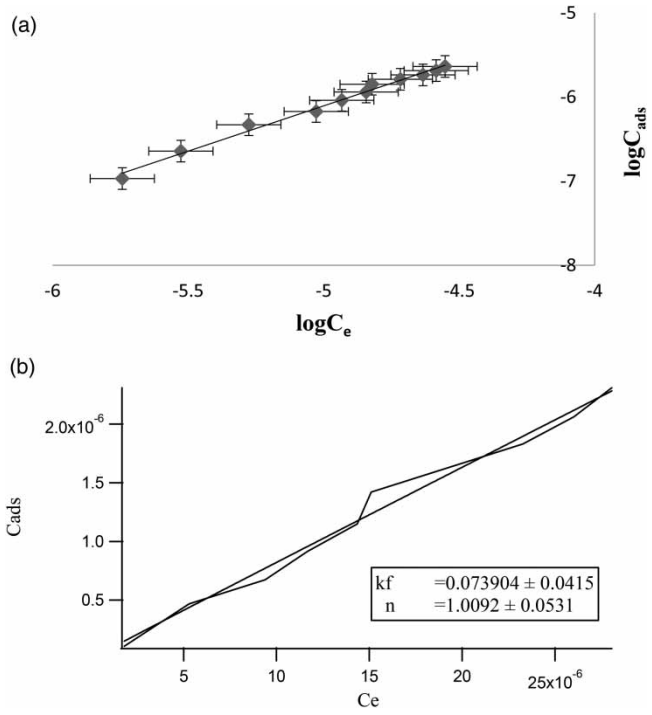

Figure 16 | (a) Freundlich isotherm's linear plot for removal of CR onto CLPP. (b) Freundlich isotherm's non-linear plot for removal of CR onto CLPP.

4.9.3. Temkin isotherm model

Based on the Temkin isothermal model, when adsorption is characterized by a homogeneous spread of absorption energies, thermal adsorption of all molecules reduces linearly as the covering of the adsorbent surface increases. Equation (12) can be used to represent the Temkin isotherm:

$$Q_e = \frac{RT}{b_T} \ln (A_T C_e) = \frac{RT}{b_T} \ln (A_T) + \frac{RT}{b_T} \ln (C_e) \tag{12}$$

where A_T is the Temkin isotherm equilibrium binding constant (L g^{-1}); b_T is the Temkin isotherm constant; C_e is the equilibrium concentration (mg L^{-1}); Q_e is the equilibrium quantity of adsorbate in the adsorbent (mg g^{-1}); R is the general gas constant (8.314 J $mol^{-1}K^{-1}$); and T is the temperature in kelvin (K) (Yaneva & Georgieva 2012).

The Temkin adsorption isotherm has the advantage of allowing the heat of adsorption to be calculated; the adsorption mechanism is exothermic if constant b_T is positive (Dada *et al.* 2012). The value of $R^2 = 0.885$ is the relatively low compared to the other isotherms adsorption models. As a result, it does not provide the greatest

fitting for the study's experimental results. Supplementary Table S13 contains the experimental data, and Figure 17(a) and 17(b) shows the linear graph and the non-linear plots, respectively.

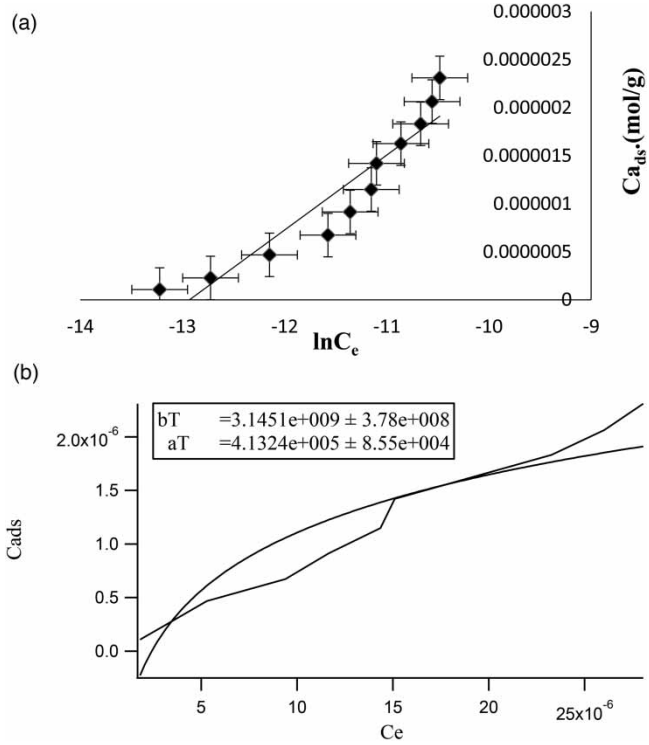

Figure 17 | (a) Temkin isotherm's linear plot for removal of CR onto CLPP. (b) Temkin isotherm's non-linear plot for removal of CR onto CLPP.

4.9.4. Dubinin–Radushkevich isotherm model

The Dubinin–Radushkevich (D-R) adsorption isotherm model was proposed for the influence of the adsorbent's porous structure. Based on adsorption theory, it was thought that micro-pore area filling was related to adsorption rather than layer-by-layer adsorption on the porous wall (Javed *et al.* 2017a). High solute activity and intermediate concentrations are good candidates for the D-R model. The D-R equation's linear version may be written as:

$$\ln Q_e = \ln A_s + \beta\varepsilon^2 \tag{13}$$

Here Q_e is the equilibrium quantity of adsorbate in the adsorbent (mg g^{-1}), D-R isotherm constant is represented by β (mol^2 K J^{-2}); A_s represents the hypothetical isotherm adsorption capacity (mg g^{-1}); and ε is the Polanyi potential and is expressed in Equation (14):

$$\varepsilon = RT\ln\left(1+\frac{1}{C_e}\right) \tag{14}$$

The integral form of the D-R isothermal equation is:

$$\ln C_{ads} = \ln C_m - \beta\varepsilon^{-2} \tag{15}$$

To find the energy of adsorption mechanism (E_s), the value of β is used:

$$E_s = \frac{1}{(-2\beta)^{1/2}} \tag{16}$$

The average free energy flow from the dye to the adsorbent's surface is indicated here by E_s. Additionally, it appears that the exclusion of CR dye is the mechanism of physical adsorption demonstrating from the value of E_s obtained from Equation (16) of the D-R isotherm ($E_s = 0.064$ kJ mol^{-1}). The value of free sorption energy increases with the strength of the bond between the adsorbent and adsorbate. In most cases, the D-R model is employed to distinguish between physical and chemical adsorption mechanisms (Javed *et al.* 2017a). The straight-line plot and the correlation factor ($R^2 = 0.9927$) demonstrate that experimental data (presented in Supplementary Table S14, and Figure 18(a)) obeyed the D-R adsorption isotherm model completely (Yaneva & Georgieva 2012). The D-R isotherm's non-linear plot for adsorption of CR dye molecules is presented in Figure 18(b).

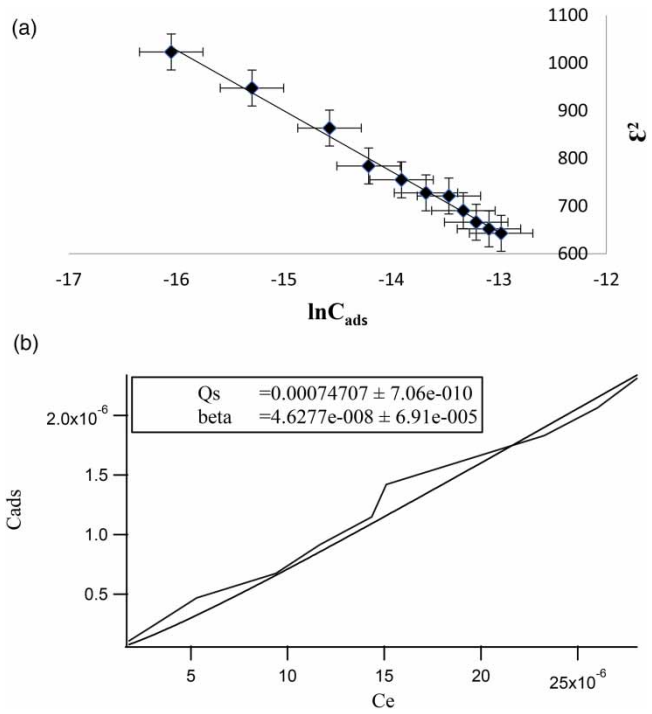

Figure 18 | (a) Dubinin–Radushkevich isotherm's linear plot for removal of CR onto CLPP. (b) Dubinin–Radushkevich isotherm's non-linear plot for removal of CR onto CLPP.

The experimental results are best explained by the Freundlich and D-R isotherms, as demonstrated by the determination coefficient in accordance with the graphical depiction and Table 3 listing of the parameters of different isotherms. The slope coefficient for the Langmuir adsorption isotherm model is 0.9891, which is less than the slope coefficient for the Freundlich isotherm model. This difference confirms that the data fits best the Freundlich isotherm model, according to which CR adsorption takes place on the heterogeneous surface of the CLPP. Additionally, a value of n larger than one implies that the procedure of CR adsorption onto CLPP is beneficial, and the calculated value of E_s indicates the physical adsorption. The operating conditions used in the adsorption mechanism (pH, initial concentration, amount of adsorbent, etc.) and the characteristics of the adsorbent determined the adsorption capacity. A comparison of adsorption capacity of different adsorbents for the removal of CR is given in Table 4. The parameter employed for comparison is the adsorption capacity. The value of adsorption capacity, which is in good alignment with the results of the majority of previously published research, suggests that CR might be easily adsorbed on the CLPP developed in this study.

4.10. ARE error analysis

The feasibility of adsorption isotherm and adsorption kinetic models was validated using certain error function. The error function investigated in this case was 'the average relative error'. The fractional error distribution throughout the whole detection limit is minimized by this error function, which has the following expression:

$$\mathrm{ARE} = \frac{n}{100} \sum_{i=1}^{n} \left| \frac{Q_{e(cal)} - Q_{e\,(exp)}}{Q_{e(exp)}} \right| \tag{17}$$

Table 4 | Comparison of adsorption capacity of various adsorbents for Congo red dye removal

Adsorbent	Maximum adsorption capacity(mg g^{-1})	Reference
Banana peel powder	1.721	Mondal & Kar (2018)
Durian peel powder	107.52	Kamsonlian *et al.* (2013)
Solanum tuberosum peel	6.9	Rehman *et al.* (2018)
Peanut shell	15.09	Abbas *et al.* (2012)
Sugarcane bagasse	38.2	Zhang *et al.* (2011)
Orange peel powder	11.919	Harnal *et al.* (2020)
Tea waste	3	Foroughi-dahr *et al.* (2016)
Powdered eggshell	95.25	Zulfikar & Setiyanto (2013)
Cedrus deodara sawdust	182.5	Muneer *et al.* (2021)
Aloe vera leaves shell	1,850	Khaniabadi *et al.* (2017)
Citrus limetta peel powder	5.2742	Present study

where $Q_{e(cal)}$ and $Q_{e(exp)}$ are calculated and experimental values of initial adsorbate concentration in solid state, respectively and 'n' is the number of valuable observation. The larger the value of R^2 and the smaller the value of an adsorption isotherm or kinetic model's error function, the better fit that model is to adsorption data (Batool *et al.* 2018; Alrobei *et al.* 2021).

The outcomes of ARE error analysis for various adsorption isotherms and adsorption kinetic models are presented in Table 5. The results showed that, compared to other adsorption isotherms and kinetic models, the values of the ARE error analysis for the Freundlich isotherm and the pseudo-second-order kinetic model are smaller (although the values of the regression coefficients, i.e., R^2 are greater). It was revealed that the Freundlich and pseudo-second-order kinetic models were appropriate for this adsorption process.

Table 5 | ARE error analysis values of adsorption isotherm and adsorption kinetic models

Isotherm models	(i) Langmuir isotherm model	2.64×10^{14}
	(ii) Freundlich isotherm model	1.06×10^{09}
	(iii) Temkin isotherm model	1.61×10^{16}
	(iv) Dubinin–Radushkevich isotherm	2.43×10^{10}
Kinetic models	(i) Pseudo-first-order	−60.74977625
	(ii) Pseudo-second-order	−98.60786052
	(iii) Intraparticle diffusion model	−97.20220512
	(iv) Liquid film model	−97.8442112

4.11. Thermodynamic of adsorption

The thermodynamic characteristics, such as Gibbs free energy, might be used to study the viability and kind of adsorption. By plotting ln K_c in contrast to $1/T$, a straight-line graph is obtained. The graph's slope is ΔH, while its intercept is ΔS. Where R denotes the general gas constant, and its value is 8.31 J $mol^{-1}K^{-1}$, and T denotes the temperature in Kelvin.

The relation of ΔG is given in Equation (18):

$$\Delta G = \Delta H - T\Delta S^{o} \tag{18}$$

The Van't Hoff equation, which has the following formula as an alternative form, is used to get the values of ΔH and ΔS^{o}:

$$\ln K_c = \frac{\Delta S^{o}}{R} - \frac{\Delta H}{RT} \tag{19}$$

where K_c is the constant of equilibrium, for sorption, R is the universal gas constant, and T is the temperature in kelvin (K). The value K_c can be obtained by the given relation:

$$K_c = \frac{C_{ads}}{C_e} \tag{20}$$

Adsorbate molecules and adsorbent interactions can be categorized according to the quantity of entropy change (ΔS^o) and enthalpy change (ΔH^o). Enthalpy (ΔH^o) and entropy (ΔS^o) at various temperatures were calculated using the slope and intercept of the ln K_c versus $1/T$ plot. Figure 19 depicts the Van't Hoff plot graph. As the temperature rises from 298 to 338 K, the −ve value of ΔG^o increases, indicating that the adsorption process is more feasible and spontaneous, resulting in better CR sorption capability on CLPP. Because the value of free energy (ΔG^o) reduces with rising temperature, the adsorption process becomes more spontaneous (He *et al.* 2010). It is clear that the adsorption of CR on CLPP is an exothermic process with negative ΔH values since the values of adsorption capacity decrease as temperature rises (shown in Table 6). This may be due to reduced binding forces between the dye molecules and the active sites of adsorbent (Litefti *et al.* 2019). A positive ΔS^o value reveals that the adsorption method is based on a separation mechanism (Oyekanmi *et al.* 2021). Statistical results for the thermodynamic adsorption are summarized in Supplementary Table S15.

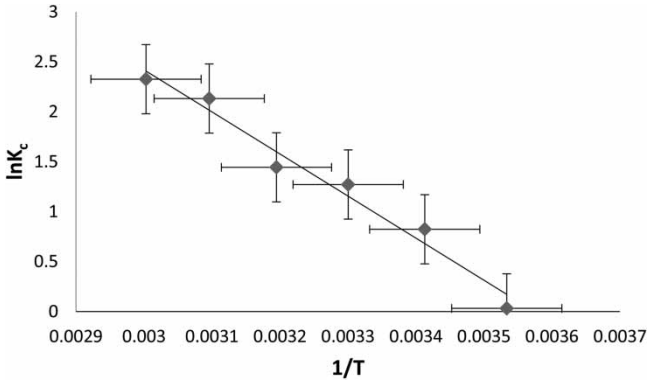

Figure 19 | Van't Hoff plot for adsorption of CR onto CLPP.

Table 6 | Calculated thermodynamic adsorption parameters

ΔG K J mol^{-1}	ΔH K J mol^{-1}	ΔS J mol^{-1}K^{-1}
1.6375		
−0.0779		
−2.0062		
−3.0973	−37.378	0.133
−3.5164		
−5.1942		
−5.6659		

4.12. Adaptation of the procedure with tap water

Tap water was used to test the suggested procedure's applicability (Javed *et al.* 2017b; Batool *et al.* 2021). The experiment was performed under optimized conditions (pH = 6.0, adsorbent dosage = 0.4 g, contact period = 90 min, starting dye concentration = 10 ppm, temperature = 60 °C) to investigate the potential of CLPP for the removal of Congo red dye. According to the results, 82% of the color was removed. The results proved that the employed process is applicable to normal water samples (Naushad *et al.* 2016).

5. BIOSORPTION MECHANISM

Electrostatic interactions and hydrogen bonds have mostly influenced the biosorption adsorption method for the CR dye molecule. Different functional groups such as −OH, −COOR, C − O − C, and −COOH groups were prominent on the surface of the *C. limetta* peels, according to FTIR spectra. After the adsorption of CR dye, FTIR peaks move (8 to 22 cm^{-1}) in the direction of –OH and –COOH groups were found in the spectra, indicating that such groups were primarily applicable for CR dye adsorption onto the surface of *C. limetta* peels. Water molecules in which adsorbent and adsorbate is present dissociates into H^+ and OH^- ions. CR dye contain O^-Na^+ group, OH^- group, which dissociates from water electrostatically attracts sodium ions to form NaOH leaving O^- ions. The carboxylic or hydroxylic groups present on the surface of CLPP consume H^+ by protonation, forming positively charged $-OH_2^+$ and $-COOH_2^+$ molecules that combine with O^- group of CR dye through an electrostatic effect to adsorb CR dye (Yang *et al.* 2019).

$$CLPP - COOH + H^+ \rightarrow CLPP - COOH_2^+ \tag{21}$$

Also,

$$CLPP - OH + H^+ \rightarrow CLPP - OH_2^+ \tag{22}$$

$$CR - O^-Na^+ + OH^- \rightarrow CR - O^- + NaOH \tag{23}$$

$$CR - O^- + CLPP - OH_2^+ \rightarrow CLPP - O - CR + H_2O \tag{24}$$

Also,

$$CLPP - COOH_2^+ + CR - O^- \rightarrow CLPP - COO - CR + H_2O \tag{25}$$

The pH of the adsorbate has an impact on the active site of the biosorption system. The pH of the solution has a substantial impact on the physical interaction of dye molecules on the binding sites of the absorbent. The highest adsorption capacity of Congo red dyes on *C. limetta* peels was noticed in this research when the solution was acidic (pH 6). *C. limetta* peels had a positively charged surface characteristics at an acidic pH and many protonated sites (H^+) on the surfaces, which increased the electrostatic interaction between the negatively charged CR dye molecules and the positively charged surface of the CLPP. Additionally, at a basic pH, CLPP's surface had many hydroxyl ions (OH), which led to the deprotonation, of the –COOH and –OH groups. This may decrease the electrostatic force between the positively surface charge of the *C. limetta* peel and the negatively charged CR dye molecules. CR dye adsorption onto the CLPP favored H-bonding and $\pi - \pi$ interaction in addition to electrostatic attraction (Oyekanmi *et al.* 2021).

Isotherm studies revealed that the D-R and Freundlich models best illustrated experimental data regarding the adsorption of CR dye molecules on the surface of CLPP, suggesting that multilayer adsorption takes place on a miscellaneous surface enriched with negative ions for the adsorption process.

6. DESORPTION

Recovery of adsorbent (CLPP) and adsorbate (Alrobei *et al.* 2021) are salient features of wastewater treatment because it demonstrate that this technique is inexpensive. Using sodium hydroxide (NaOH) as a desorbing agent, desorption test was performed to determine whether the CLPP adsorbent can be reused (Javed *et al.* 2017a; Dai *et al.* 2019; Lafi *et al.* 2019). In the experiment, a specific quantity (0.4 g) of CLPP adsorbent containing dye was agitated with 0.01 M NaOH for 25 min. According to the experiment's results (Supplementary Table S16), 80% of the adsorbent was regenerated, making it suitable for use in further adsorption procedures.

7. CONCLUSION

- CLPP has an efficient and appropriate adsorption process for removing harmful, toxic synthetic dyes. The adsorption process of CR was significant within the range investigated. The optimum conditions for 88.2% adsorption of CR were pH 6, 0.4 g of adsorbent dose, 90 min contact time, and initial concentration of 10 ppm within 60 °C.

- Different kinetic models, such as pseudo-first-order, pseudo-second-order, and intraparticle diffusion models, as well as the liquid film model, have been used and debated. Kinetic data was better fitted to the pseud-second-order kinetic model as the value of slope coefficient (R^2) is 0.9918 and $Q_{e(cal)} = 0.206$ mg g^{-1}, which is very close to the experimental $Q_{e(exp)} = 0.191$ mg g^{-1}.
- The appropriate isotherm model for the adsorption process was selected after examining concentration data from the experiment using a number of isotherm models. In this investigation, the Langmuir, Freundlich, Temkin, and D-R isotherm models were adopted. The Freundlich and D-R isotherm models best described the biosorption process since their slope coefficient (R^2) value is 0.99, which is close to unity, and their ARE error analysis has a lower value.
- Overall, the thermodynamic characteristics demonstrated that CR dye adsorption on CLPP was spontaneous, exothermic, and dependent on physical forces.
- The FTIR analysis identified a transition in the –OH and –COOH groups, predicting that these groups were mainly in charge of CR dye adsorption C. limetta peel surfaces.
- The established technique was 82% applicable with tap water, and the desorption experiment resulted in an 80% regeneration of the adsorbent, indicating that it may be reused for adsorption. *C. limetta* peels may be employed as a competitive adsorbent for the removal of pollutants from the textiles and coloring industries due to the remarkable removal capacity of CR dyes.

ACKNOWLEDGEMENTS

First and foremost, all praise to Allah, the Almighty, the Most Merciful, for His blessings given to me during my study and in completing this work. I would like to offer my heartfelt appreciation and sincere thanks to my beloved parents, family, and friends for their prayers, support, and encouragement. In addition, my greatest gratitude and appreciation are addressed to my supervisor, Dr Tariq Javed, Lecturer, Department of Chemistry, University of Sahiwal, Sahiwal, Punjab, Pakistan, who has given me his valuable guidance, advice, and encouragement so I could complete this work in time.

FUNDING

No funding was allocated for the study's accomplishment.

DATA TRANSPARENCY STATEMENT

The authors will assure data transparency.

AUTHORS' CONTRIBUTIONS

All authors contributed equally to this research study. The final manuscript was evaluated and approved by all authors.

DATA AVAILABILITY STATEMENT

All relevant data are included in the paper or its Supplementary Information.

CONFLICT OF INTEREST

The authors declare there is no conflict.

REFERENCES

Abbas, A., Murtaza, S., Shahid, K., Munir, M., Ayub, R. & Akber, S. 2012 Comparative study of adsorptive removal of Congo red and brilliant green dyes from water using peanut shell. *Middle-East Journal of Scientific Research* **11**(6), 828–832.

Akpomie, K. G. & Conradie, J. 2020 Banana peel as a biosorbent for the decontamination of water pollutants: a review. *Environmental Chemistry Letters* **18**(4), 1085–1112.

Ali, M. A., Mubarak, M. F., Keshawy, M., Zayed, M. A. & Ataalla, M. 2022 Adsorption of Tartrazine anionic dye by novel fixed bed Core-Shell-polystyrene Divinylbenzene/Magnetite nanocomposite. *Alexandria Engineering Journal* **61**(2), 1335–1352. https://doi.org/10.1016/j.aej.2021.06.016.

Alrobei, H., Prashanth, M., Manjunatha, C., Kumar, C. P., Chitrabanu, C., Shivaramu, P. D., Kumar, K. Y. & Raghu, M. 2021 Adsorption of anionic dye on eco-friendly synthesised reduced graphene oxide anchored with lanthanum aluminate:

isotherms, kinetics and statistical error analysis. *Ceramics International* **47**(7), 10322–10331. https://doi.org/10.1016/j.ceramint.2020.07.251.

Al-Tohamy, R., Ali, S. S., Li, F., Okasha, K. M., Mahmoud, Y. A.-G., Elsamahy, T., Jiao, H., Fu, Y. & Sun, J. 2022 A critical review on the treatment of dye-containing wastewater: ecotoxicological and health concerns of textile dyes and possible remediation approaches for environmental safety. *Ecotoxicology and Environmental Safety* **231**, 113160. https://doi.org/10.1016/j.ecoenv.2021.113160.

Alwared, A. I., Al-Musawi, T. J., Muhaisn, L. F. & Mohammed, A. A. 2021 The biosorption of reactive red dye onto orange peel waste: a study on the isotherm and kinetic processes and sensitivity analysis using the artificial neural network approach. *Environmental Science and Pollution Research* **28**(3), 2848–2859. https://doi.org/10.1007/s11356-020-10613-6.

Anah, L. & Astrini, N. 2018 Isotherm adsorption studies of Ni (II) ion removal from aqueous solutions by modified carboxymethyl cellulose hydrogel. In *IOP Conference Series: Earth and Environmental Science*. IOP Publishing, p. 012017.

Batool, F., Akbar, J., Iqbal, S., Noreen, S. & Bukhari, S. N. A. 2018 Study of isothermal, kinetic, and thermodynamic parameters for adsorption of cadmium: an overview of linear and nonlinear approach and error analysis. *Bioinorganic Chemistry and Applications* **2018**. http://dx.doi.org/10.1155/2018/3463724.

Batool, M., Javed, T., Wasim, M., Zafar, S. & Din, M. I. 2021 Exploring the usability of *Cedrus deodara* sawdust for decontamination of wastewater containing crystal violet dye. *Desalination and Water Treatment* 2021, **224**, p. 433–448. http://doi.org/10.5004/dwt.2021.27192.

Bhattacharyya, K. G. & Sharma, A. 2004 *Azadirachta indica* leaf powder as an effective biosorbent for dyes: a case study with aqueous Congo Red solutions. *Journal of Environmental Management* **71**(3), 217–229. https://doi.org/10.1016/j.jenvman.2004.03.002.

Buvaneswari, K. & Singanan, M. 2020 Review on scanning electron microscope analysis and adsorption properties of different activated carbon materials. *Materials Today: Proceedings*. https://doi.org/10.1016/j.matpr.2020.09.426.

Chai, W. S., Cheun, J. Y., Kumar, P. S., Mubashir, M., Majeed, Z., Banat, F., Ho, S.-H. & Show, P. L. 2021 A review on conventional and novel materials towards heavy metal adsorption in wastewater treatment application. *Journal of Cleaner Production* **296**, 126589. https://doi.org/10.1016/J.JCLEPRO.2021.126589.

Chen, X. 2015 Modeling of experimental adsorption isotherm data. *Information* **6**(1), 14–22. https://doi.org/10.3390/info6010014.

Chuah, T. G., Jumasiah, A., Azni, I., Katayon, S. & Choong, S. T. 2005 Rice husk as a potentially low-cost biosorbent for heavy metal and dye removal: an overview. *Desalination* **175**(3), 305–316. https://doi.org/10.1016/j.desal.2004.10.014.

Dada, A., Olalekan, A., Olatunya, A. & Dada, O. 2012 Langmuir, Freundlich, Temkin and Dubinin–Radushkevich isotherms studies of equilibrium sorption of Zn^{2+} unto phosphoric acid modified rice husk. *IOSR Journal of Applied Chemistry* **3**(1), 38–45.

Dai, Y., Zhang, N., Xing, C., Cui, Q. & Sun, Q. 2019 The adsorption, regeneration and engineering applications of biochar for removal organic pollutants: a review. *Chemosphere* **223**, 12–27. https://doi.org/10.1016/j.chemosphere.2019.01.161.

El-Ahmady, E.-N. N., Rabei, N. H. & El-Malkey, S. E. 2020 Eco-friendly approach for biosorption of Pb^{2+} and carcinogenic Congo red dye from binary solution onto sustainable *Ulva lactuca* biomass. *Scientific Reports* **10**(1), 1–22.

Felista, M. M., Wanyonyi, W. C. & Ongera, G. 2020 Adsorption of anionic dye (Reactive black 5) using macadamia seed husks: kinetics and equilibrium studies. *Scientific African* **7**, e00283. https://doi.org/10.1016/j.sciaf.2020.e00283.

Foroughi-dahr, M., Esmaieli, M., Abolghasemi, H., Shojamoradi, A. & Sadeghi Pouya, E. 2016 Continuous adsorption study of Congo red using tea waste in a fixed-bed column. *Desalination and Water Treatment* **57**(18), 8437–8446. https://doi.org/10.1080/19443994.2015.1021849.

Guo, X., Kong, L., Ruan, Y., Diao, Z., Shih, K., Su, M. & Chen, D. 2020 Green and facile synthesis of cobalt-based metal–organic frameworks for the efficient removal of Congo red from aqueous solution. *Journal of Colloid and Interface Science* **578**, 500–509. https://doi.org/10.1016/j.jcis.2020.05.126.

Harnal, V. S., Darla, U. & Lataye, D. H. 2020 Removal of Congo red dye from wastewater using orange peel as an adsorbent. *Journal of Indian Association for Environmental Management (JIAEM)* **40**(2), 52–59.

He, J., Hong, S., Zhang, L., Gan, F. & Ho, Y.-S. 2010 Equilibrium and thermodynamic parameters of adsorption of methylene blue onto rectorite. *Fresenius Environmental Bulletin* **19**(11), 2651–2656.

Imran, M. S., Javed, T., Areej, I. & Haider, M. N. 2022 Sequestration of crystal violet dye from wastewater using low-cost coconut husk as a potential adsorbent. *Water Science and Technology* **85**(8), 2295–2317. https://doi.org/10.2166/wst.2022.124.

Javed, T., Khalid, N. & Mirza, M. L. 2017a Adsorption characteristics of copper ions on low-rank Pakistani coal. *Desalination and Water Treatment* **59**, 181–190. http://dx.doi.org/10.5004/dwt.2017.1265.

Javed, T., Khalid, N. & Mirza, M. L. 2017b Kinetics, equilibrium and thermodynamics of cerium removal by adsorption on low-rank coal. *Desalination and Water Treatment* **89**, 240–249. http://dx.doi.org/10.5004/dwt.2017.21357.

Kamsonlian, S., Suresh, S., Majumder, C. & Chand, S. 2013 Biosorption of arsenic by mosambi (*Citrus limetta*) peel: equilibrium, kinetics, thermodynamics and desorption study. *Asian Journal of Chemistry* **25**(5), 2409. http://dx.doi.org/10.14233/ajchem.2013.13336.

Karaman, C., Karaman, O., Show, P.-L., Karimi-Maleh, H. & Zare, N. 2022 Congo red dye removal from aqueous environment by cationic surfactant modified-biomass derived carbon: equilibrium, kinetic, and thermodynamic modeling, and forecasting via artificial neural network approach. *Chemosphere* **290**, 133346. https://doi.org/10.1016/j.chemosphere.2021.133346.

Khan, S. & Malik, A. 2014 Environmental and health effects of textile industry wastewater. In: *Environmental Deterioration and Human Health*. Springer, Dordrecht, Midtown Manhattan, New York City, pp. 55–71.

Khaniabadi, Y. O., Mohammadi, M. J., Shegerd, M., Sadeghi, S., Saeedi, S. & Basiri, H. 2017 Removal of Congo red dye from aqueous solutions by a low-cost adsorbent: activated carbon prepared from *Aloe vera* leaves shell. *Environmental Health Engineering and Management Journal* **4**(1), 29–35. http://dx.doi.org/10.15171/EHEM.2017.05.

Kim, G., Kang, P.-G., Kim, E. & Seo, K. 2022 Application of best available techniques to remove air and water pollutants from textile dyeing and finishing in South Korea. *Sustainability* **14**(4), 2209. https://doi.org/10.3390/su14042209.

Lafi, R., Montasser, I. & Hafiane, A. 2019 Adsorption of Congo red dye from aqueous solutions by prepared activated carbon with oxygen-containing functional groups and its regeneration. *Adsorption Science & Technology* **37**(1–2), 160–181. http://dx.doi.org/10.1177/0263617418819227.

Lellis, B., Fávaro-Polonio, C. Z., Pamphile, J. A. & Polonio, J. C. 2019 Effects of textile dyes on health and the environment and bioremediation potential of living organisms. *Biotechnology Research and Innovation* **3**(2), 275–290. https://doi.org/10.1016/j.biori.2019.09.001.

Litefti, K., Freire, M. S., Stitou, M. & González-Álvarez, J. 2019 Adsorption of an anionic dye (Congo red) from aqueous solutions by pine bark. *Scientific Reports* **9**(1), 1–11. https://doi.org/10.1038/s41598-019-53046-z.

Mondal, N. K. & Kar, S. 2018 Potentiality of banana peel for removal of Congo red dye from aqueous solution: isotherm, kinetics and thermodynamics studies. *Applied Water Science* **8**(6), 1–12. http://dx.doi.org/10.1007/s13201-018-0811-x.

Muneer, I., Javed, T., Majeed, A. A. & Masood, H. T. 2021 A brief study of adsorption of Congo red dye over sawdust of *Cedrus deodara*. *Desalination and Water Treatment* **235**, 272–282.

Nandiyanto, A. B. D., Oktiani, R. & Ragadhita, R. 2019 How to read and interpret FTIR spectroscope of organic material. *Indonesian Journal of Science and Technology* **4**(1), 97–118. https://doi.org/10.17509/ijost.v4i1.15806.

Naushad, M., Abdullah ALOthman, Z., Rabiul Awual, M., Alfadul, S. M. & Ahamad, T. 2016 Adsorption of rose Bengal dye from aqueous solution by amberlite Ira-938 resin: kinetics, isotherms, and thermodynamic studies. *Desalination and Water Treatment* **57**(29), 13527–13533. https://doi.org/10.1080/19443994.2015.1060169.

Oyekanmi, A., Ahmad, A., Mohd Setapar, S. H., Alshammari, M. B., Jawaid, M., Hanafiah, M. M., Abdul Khalil, H. & Vaseashta, A. 2021 Sustainable *Durio zibethinus*-derived biosorbents for Congo red removal from aqueous solution: statistical optimization, isotherms and mechanism studies. *Sustainability* **13**(23), 13264. https://doi.org/10.3390/su132313264.

Peñafiel, M., Matesanz, J., Vanegas, E., Bermejo, D. & Ormad, M. 2020 Corncobs as a potentially low-cost biosorbent for sulfamethoxazole removal from aqueous solution. *Separation Science and Technology* **55**(17), 3060–3071. https://doi.org/10.1080/01496395.2019.1673414.

Plazinski, W. 2010 Applicability of the film-diffusion model for description of the adsorption kinetics at the solid/solution interfaces. *Applied Surface Science* **256**(17), 5157–5163. https://doi.org/10.1016/j.apsusc.2009.12.083.

Rani, S. & Chaudhary, S. 2022 Adsorption of methylene blue and crystal violet dye from wastewater using *Citrus limetta* peel as an adsorbent. *Materials Today: Proceedings* **60**, 336–344. https://doi.org/10.1016/j.matpr.2022.01.237.

Rehman, R., Manzoor, I. & Mitu, L. 2018 Isothermal study of Congo red dye biosorptive removal from water by *Solanum tuberosum* and *Pisum sativum* peels in economical way. *Bulletin of the Chemical Society of Ethiopia* **32**(2), 213–223. https://doi.org/10.4314/bcse.v32i2.3.

Sahmoune, M. N. 2019 Evaluation of thermodynamic parameters for adsorption of heavy metals by green adsorbents. *Environmental Chemistry Letters* **17**(2), 697–704.

Samsami, S., Mohamadizaniani, M., Sarrafzadeh, M.-H., Rene, E. R. & Firoozbahr, M. 2020 Recent advances in the treatment of dye-containing wastewater from textile industries: overview and perspectives. *Process Safety and Environmental Protection* **143**, 138–163. https://doi.org/10.1016/j.psep.2020.05.034.

Sarker, T. C., Azam, S. M. G. G., El-Gawad, A. M. A., Gaglione, S. A. & Bonanomi, G. 2017 Sugarcane bagasse: a potential low-cost biosorbent for the removal of hazardous materials. *Clean Technologies and Environmental Policy* **19**(10), 2343–2362.

Shakoor, S. & Nasar, A. 2016 Removal of methylene blue dye from artificially contaminated water using *Citrus limetta* peel waste as a very low cost adsorbent. *Journal of the Taiwan Institute of Chemical Engineers* **66**, 154–163. https://doi.org/10.1016/j.jtice.2016.06.009.

Shakoor, S. & Nasar, A. 2018 Utilization of *Punica granatum* peel as an eco-friendly biosorbent for the removal of methylene blue dye from aqueous solution. *Journal of Applied Biotechnology & Bioengineering* **5**(4), 242–249. https://doi.org/10.15406/jabb.2018.05.00145.

Sharma, S. & Kaur, A. 2018 Various methods for removal of dyes from industrial effluents – a review. *Indian Journal of Science and Technology* **11**(1). http://dx.doi.org/10.17485/ijst/2018/v11i12/120847.

Silva, L. M., Muñoz-Peña, M. J., Domínguez-Vargas, J. R., González, T. & Cuerda-Correa, E. M. 2021 Kinetic and equilibrium adsorption parameters estimation based on a heterogeneous intraparticle diffusion model. *Surfaces and Interfaces* **22**, 100791. https://doi.org/10.1016/j.surfin.2020.100791.

Sultana, S., Islam, K., Hasan, M. A., Khan, H. J., Khan, M. A. R., Deb, A., Al Raihan, M. & Rahman, M. W. 2022 Adsorption of crystal violet dye by coconut husk powder: isotherm, kinetics and thermodynamics perspectives. *Environmental Nanotechnology, Monitoring & Management* **17**, 100651. https://doi.org/10.1016/j.enmm.2022.100651.

Suryavanshi, U. & Shukla, S. R. 2010 Adsorption of Pb^{2+} by alkali-treated *Citrus limetta* peels. *Industrial & Engineering Chemistry Research* **49**(22), 11682–11688. https://doi.org/10.1021/ie101491w.

Swan, N. B. & Zaini, M. A. A. 2019 Adsorption of malachite green and Congo red dyes from water: recent progress and future outlook. *Ecological Chemistry and Engineering* **26**(1), 119–132. http://dx.doi.org/10.1515/eces-2019-0009.

Tiernan, H., Byrne, B. & Kazarian, S. G. 2020 ATR-FTIR spectroscopy and spectroscopic imaging for the analysis of biopharmaceuticals. *Spectrochimica Acta Part A: Molecular and Biomolecular Spectroscopy* **241**, 118636. https://doi.org/10.1016/j.saa.2020.118636.

Wang, Y. & Chu, W. 2011 Adsorption and removal of a xanthene dye from aqueous solution using two solid wastes as adsorbents. *Industrial & Engineering Chemistry Research* **50**(14), 8734–8741. https://doi.org/10.1021/ie1024497.

Wang, L. & Wang, A. 2008 Adsorption properties of Congo red from aqueous solution onto surfactant-modified montmorillonite. *Journal of Hazardous Materials* **160**(1), 173–180. https://doi.org/10.1016/j.jhazmat.2008.02.104.

Wekoye, J. N., Wanyonyi, W. C., Wangila, P. T. & Tonui, M. K. 2020 Kinetic and equilibrium studies of Congo red dye adsorption on cabbage waste powder. *Environmental Chemistry and Ecotoxicology* **2**, 24–31. https://doi.org/10.1016/j.enceco.2020.01.004.

Yaneva, Z. L. & Georgieva, N. V. 2012 Insights into Congo red adsorption on agro-industrial materials – spectral, equilibrium, kinetic, thermodynamic, dynamic and desorption studies. A review. *International Review of Chemical Engineering* **4**(2), 127–146.

Yang, X., Wan, Y., Zheng, Y., He, F., Yu, Z., Huang, J., Wang, H., Ok, Y. S., Jiang, Y. & Gao, B. 2019 Surface functional groups of carbon-based adsorbents and their roles in the removal of heavy metals from aqueous solutions: a critical review. *Chemical Engineering Journal* **366**, 608–621. https://doi.org/10.1016%2Fj.cej.2019.02.119.

Zafar, S., Khan, M. I., Khraisheh, M., Lashari, M. H., Shahida, S., Azhar, M. F., Prapamonthon, P., Mirza, M. L. & Khalid, N. 2019 Kinetic, equilibrium and thermodynamic studies for adsorption of nickel ions onto husk of *Oryza sativa*. *Desalination and Water Treatment* **167**, 277–290. http://dx.doi.org/10.5004/dwt.2019.24646.

Zhang, Z., Moghaddam, L., O'Hara, I. M. & Doherty, W. O. 2011 Congo red adsorption by ball-milled sugarcane bagasse. *Chemical Engineering Journal* **178**, 122–128. https://doi.org/10.1016/j.cej.2011.10.024.

Zulfikar, M. A. & Setiyanto, H. 2013 Study of the adsorption kinetics and thermodynamic for the removal of Congo red from aqueous solution using powdered eggshell. *International Journal of ChemTech Research* **5**(4), 1671–1678. https://doi.org/10.1016/j.crgsc.2021.100180.

First received 6 October 2022; accepted in revised form 20 April 2023. Available online 4 May 2023